Low Diffusive Methane Emissions From the Main Channel of a Large Amazonian Run-of-the-River Reservoir Attributed to High Methane Oxidation

Article *in* Frontiers in Environmental Science · April 2021

DOI: 10.3389/fenvs.2021.655455

CITATIONS
0

READS
29

6 authors, including:

Henrique Sawakuchi
Linköping University
59 PUBLICATIONS **880** CITATIONS
SEE PROFILE

David T Bastviken
Linköping University
193 PUBLICATIONS **10,532** CITATIONS
SEE PROFILE

Alex Enrich-Prast
Linköping University
137 PUBLICATIONS **3,361** CITATIONS
SEE PROFILE

Nicholas D. Ward
Pacific Northwest National Laboratory
97 PUBLICATIONS **1,288** CITATIONS
SEE PROFILE

frontiers in Environmental Science

ORIGINAL RESEARCH
published: 08 April 2021
doi: 10.3389/fenvs.2021.655455

Low Diffusive Methane Emissions From the Main Channel of a Large Amazonian Run-of-the-River Reservoir Attributed to High Methane Oxidation

Henrique O. Sawakuchi[1], David Bastviken[1], Alex Enrich-Prast[1], Nicholas D. Ward[2,3], Plínio B. Camargo[4] and Jeffrey E. Richey[3]*

[1] Department of Thematic Studies–Environmental Change, Linköping University, Linköping, Sweden, [2] Marine and Coastal Research Laboratory, Pacific Northwest National Laboratory, Sequim, WA, United States, [3] School of Oceanography, University of Washington, Seattle, WA, United States, [4] Center of Nuclear Energy in Agriculture, University of São Paulo, Piracicaba, Brazil

OPEN ACCESS

Edited by:
Shaoda Liu,
Beijing Normal University, China

Reviewed by:
Xiaoke Wang,
Research Center for Eco-Environmental Sciences (CAS), China
Vincent Chanudet,
Electricité de France, France

***Correspondence:**
Henrique O. Sawakuchi
henrique.sawakuchi@liu.se

Specialty section:
This article was submitted to Biogeochemical Dynamics, a section of the journal Frontiers in Environmental Science

Received: *18 January 2021*
Accepted: *17 March 2021*
Published: *08 April 2021*

Citation:
Sawakuchi HO, Bastviken D, Enrich-Prast A, Ward ND, Camargo PB and Richey JE (2021) Low Diffusive Methane Emissions From the Main Channel of a Large Amazonian Run-of-the-River Reservoir Attributed to High Methane Oxidation. Front. Environ. Sci. 9:655455. doi: 10.3389/fenvs.2021.655455

The global development of hydropower dams has rapidly expanded over the last several decades and has spread to historically non-impounded systems such as the Amazon River's main low land tributaries in Brazil. Despite the recognized significance of reservoirs to the global methane (CH_4) emission, the processes controlling this emission remain poorly understood, especially in Tropical reservoirs. Here we evaluate CH_4 dynamics in the main channel and downstream of the Santo Antônio hydroelectric reservoir, a large tropical run-of-the-river (ROR) reservoir in Amazonia. This study is intended to give a snapshot of the CH_4 dynamics during the falling water season at the initial stage after the start of operations. Our results show substantial and higher CH_4 production in reservoirs' littoral sediment than in the naturally flooded areas downstream of the dam. Despite the large production in the reservoir or naturally flooded areas, high CH_4 oxidation in the main channel keep the concentration and fluxes of CH_4 in the main channel low. Similar CH_4 concentrations in the reservoir and downstream close to the dam suggest negligible degassing at the dam, but stable isotopic evidence indicates the presence of a less oxidized pool of CH_4 after the dam. ROR reservoirs are designed to disturb the natural river flow dynamics less than traditional reservoirs. If enough mixing and oxygenation remain throughout the reservoir's water column, naturally high CH_4 oxidation rates can also remain and limit the diffusive CH_4 emissions from the main channel. Nevertheless, it is important to highlight that our results focused on emissions in the deep and oxygenated main channel. High emissions, mainly through ebullition, may occur in the vast and shallow areas represented by bays and tributaries. However, detailed assessments are still required to understand the impacts of this reservoir on the annual emissions of CH_4.

Keywords: carbon, river, hydropower, methane, oxidation, aquatic, greenhouse gas

INTRODUCTION

Hydroelectric reservoirs are recognized as an important anthropogenic source of the greenhouse gas methane (CH_4) to the atmosphere, with an estimated global flux ranging from 3 to 14 Tg CH_4 year^{-1} (Deemer et al., 2016). The number of hydropower plants emerging worldwide is steadily increasing in developed and developing nations (Zarfl et al., 2015). Until recently, the flow of the largest river in the World, the Amazon River, has been relatively unaltered. However, Brazil currently plans to continue the hydropower expansion in the Amazon basin despite the high social and environmental cost associated with the recently built dams in the Madeira and Xingu Rivers (Gerlak et al., 2020), and existing data indicates that hydroelectric reservoirs are not GHG-neutral (Wehrli, 2011; Deemer et al., 2016).

The Madeira River is one of the Amazon River's main tributaries, where two large run-of-the-river (ROR) hydropower reservoirs, Jirau and Santo Antônio, were recently built. ROR reservoirs are constructed to have a small reservoir area, low water residence time, and reduced impacts on the river channel, and in turn should have lower expected CH_4 emissions, compared to traditional reservoirs that tend to be larger, deeper, and have high water residence time (Gagnon and van de Vate, 1997). Throughout the World, this type of hydropower station is generally developed for small rivers and streams (Gagnon and van de Vate, 1997; Mallia and Lewis, 2013), and significant CH_4 emissions have already been registered for such systems in the temperate region (Delsontro et al., 2010; DelSontro et al., 2015, 2016). Although the area flooded by ROR dams is considerably smaller than what it would be as a storage type reservoir, the power density of the Santo Antônio Reservoir (11.6 MW km^2) is lower than storage reservoirs such as Segredo and Xingó Reservoirs (15.6 and 52.7 MW km^2), located in other regions of Brazil (de Faria et al., 2015; dos Santos et al., 2017). Furthermore, low land Amazonian reservoirs such as Santo Antônio have lower power density than reservoirs in high elevation and steeper areas (Almeida et al., 2019b), and because of the high temperatures throughout the year in tropical systems, high rates of CH_4 production and emission can be expected (Barros et al., 2011; Marotta et al., 2014). Recent studies have indicated minimal changes in water chemistry, thermal structure, and fine sediment transport in the Santo Antonio ROR reservoir in the Maderia River (Almeida et al., 2019a; Rivera et al., 2019), and de Araújo et al. (2019) found that CO_2 emissions in the Belo Monte ROR reservoir's main channel in the Xingu River remained similar to non-affected river areas. These findings suggest that the main channel of ROR reservoirs can keep the original river characteristics.

Despite a large amount of undergoing or planned hydropower dam construction around the globe and their importance on the global CH_4 emissions (Deemer et al., 2016), the influence of large tropical ROR reservoirs on CH_4 cycling remains unknown. Here we evaluate the impact of one of the largest ROR hydropower dams in Amazonia (de Faria et al., 2015) on the CH_4 dynamics of the reservoir's main channel. We compare the potential CH_4 production, dissolved CH_4 concentrations, river-to-atmosphere CH_4 fluxes, and methane oxidation for the area affected by the Santo Antônio reservoir with areas downstream during the falling water season at the initial stage of operation and hypothesize that ROR reservoirs alter the CH_4 emissions on the original river channel due to large inputs from flooded adjacent areas.

MATERIALS AND METHODS

Study Area and Sampling Design

The Madeira River is one of the Amazon River's main tributaries, contributing to 15% of the Amazon River's water budget and approximately 50% of its sediment discharge (Filizola and Guyot, 2009). The headwaters are located in the Andes, with a catchment area of approximately 1.4×10^6 km^2 and mean annual discharge at the mouth of 32,000 m^3 s^{-1}, placing the Madeira River among the ten largest rivers in the World (Latrubesse et al., 2005). The Madeira River has turbid waters due to the transport of a sediment load of roughly 319×10^6 tons year^{-1} (Leite et al., 2011).

The Santo Antônio reservoir is a ROR hydropower reservoir located near Porto Velho (Brazil) operating with 50 bulb turbines with bottom intake and installed capacity of 3568 MW. It started partially operating in March 2012, and during the field campaign between April and May 2013 it was operating at approximately 10% of the total capacity (ONS, 2021). The reservoir covers 422 km^2, of which 34% represents the original river channel, and 66% is the flooded land area. Three sites were selected: one site in the main channel of the Santo Antônio reservoir, located approximately 9 km upstream of the dam (Site 1), another about 3 km downstream of the dam (Site 2), and the third site 95 km downstream the dam (Site 3) (**Figure 1**). Site 1 was located right downstream of two large islands in the main channel that were flooded and also received water from large tributaries upstream, which may be sources of CH_4. Site 2, just downstream of the dam, is a constrained channel where the channel banks were covered with rocks to protect the margins from erosion due to the high water turbulence in this area. Seasonally flooded forests, locally called Igapó, surround the natural river setting at Site 3 (**Figure 1**). It is important to notice that all measurements in the reservoir (Site 1) took place in the main channel of the ROR reservoir, and primarily over the original river channel, where the whole water column was expected to be thoroughly mixed and oxic due to the short water residence time (de Faria et al., 2015). Measurements and sampling were done in 2013 between April 26 and May 03 during the beginning of the falling water season when input from marginal naturally flooded areas to the main channel was presumed to be higher than other seasons. During the sampling time, the discharge measured downstream of the dam decreased by approximately 5,500 m^3 s^{-1} (**Figure 2**).

Water samples for CH_4 concentration analysis and CH_4 flux measurements were taken on two consecutive days across the channel and at different depths. At Sites 1 and 2, the cross-channel profile consisted of three equidistant points from shore to shore, and in Site 3, measurements were made at five points along the transect (**Figure 1**). At each sampling location, with

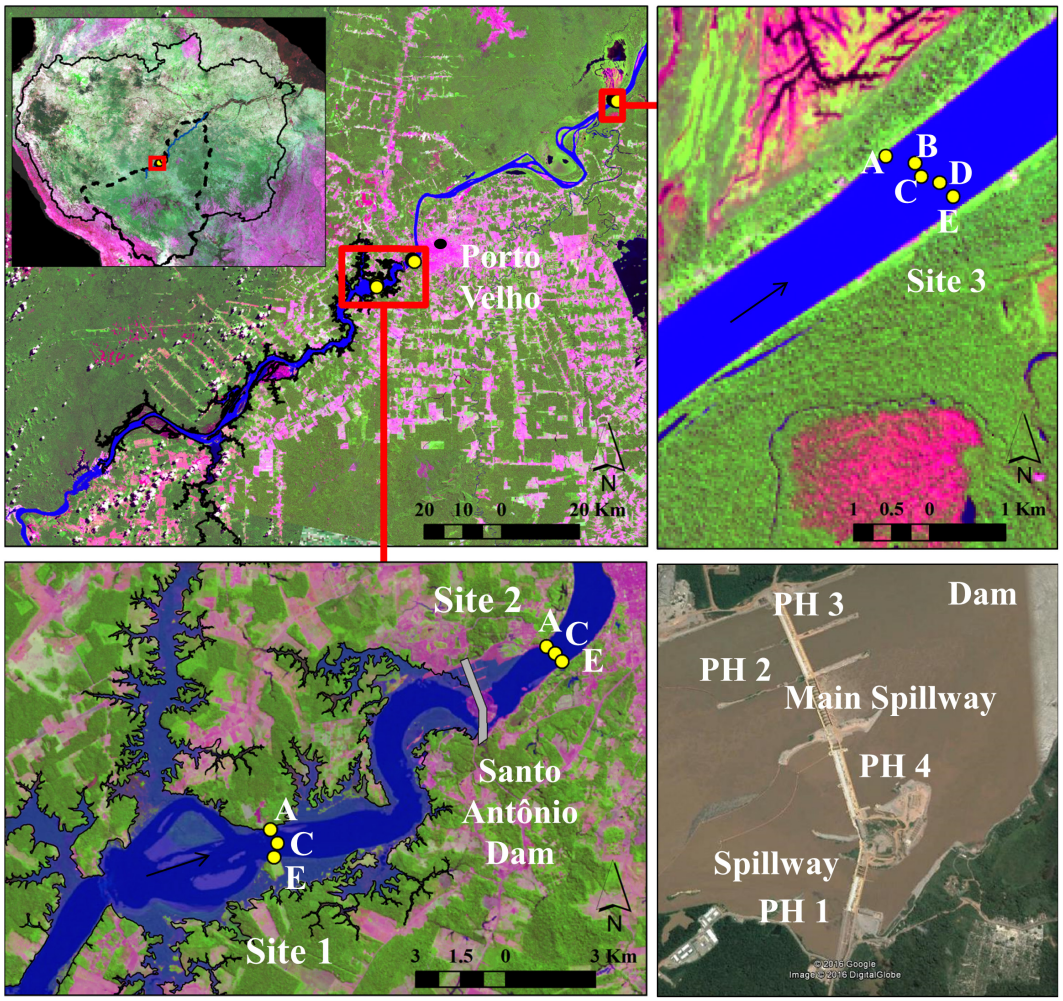

FIGURE 1 | Sampled sites in the Madeira River showing the cross-channel stations. Arrows show the flow direction. The shaded blue area shows the area flooded by the reservoir. The main background image is Landsat 8, acquired on July 10, 2013, available from USGS (https://landlook.usgs.gov/landlook/). The Santo Antônio Dam in the bottom right corner shows the Powerhouses (PH) were turbines are installed and spillways, image from Google Earth.

the boat anchored, we measured surface water physio-chemistry, wind speed, and depth. The drifting speed was registered during chamber deployments. Depth and speed were measured with a GPS/sonar (EchoMap 421, Garmin International, Inc., Olathe, KS, United States). Air temperature, atmospheric pressure, and wind speed were measured with a weather station (HOBO; Onset Computer Corporation, Bourne, MA, United States) installed on the boat, and the water temperature was measured with a pH meter (Orion 290APlus; Thermo Fisher Scientific Inc., Waltham, MA, United States). Wind speed measurements were done with the boat anchored were the drifting speed was used as a proxy for the water velocity.

Potential Methane Production and Sediment Carbon to Nitrogen Ratio

A layer of 6–10 cm sediment was collected at sites 1 and 3, using a Van Veen grab sampler. Due to the dam's high discharge, the river bed in the area after the dam (Site 2) was protected with rocks in the shore and bottom. Thus we could not sample the bottom sediment in this site. At site 1, muddy sediment was collected from the reservoirs' littoral sediment (area recently flooded by the dam), and at site 3, sediment was collected at the naturally flooded shore and at the middle of the channel, where muddy sediment and sand was found, respectively. Triplicate sediment samples were taken from each location and stored in 250 ml acid-washed plastic bottles completely filled with sediment to avoid oxygen exposure. Each bottle's sediment content was homogenized, and aliquots of 30 ml of wet sediment were transferred to 118 ml glass vials closed with butyl rubber stoppers and sealed with aluminum crimps. Four vials were prepared for each sample, totalizing 12 vials for each of the three locations. All vials were flushed with pure nitrogen (N_2) to create an anoxic environment where CH_4 can be produced. Vials were incubated in the dark without agitation at the same river water temperature (28°C) for 111 days. Analyses were done at a frequency of 3–4 days during the first 41 days, then three analyses on incubation days

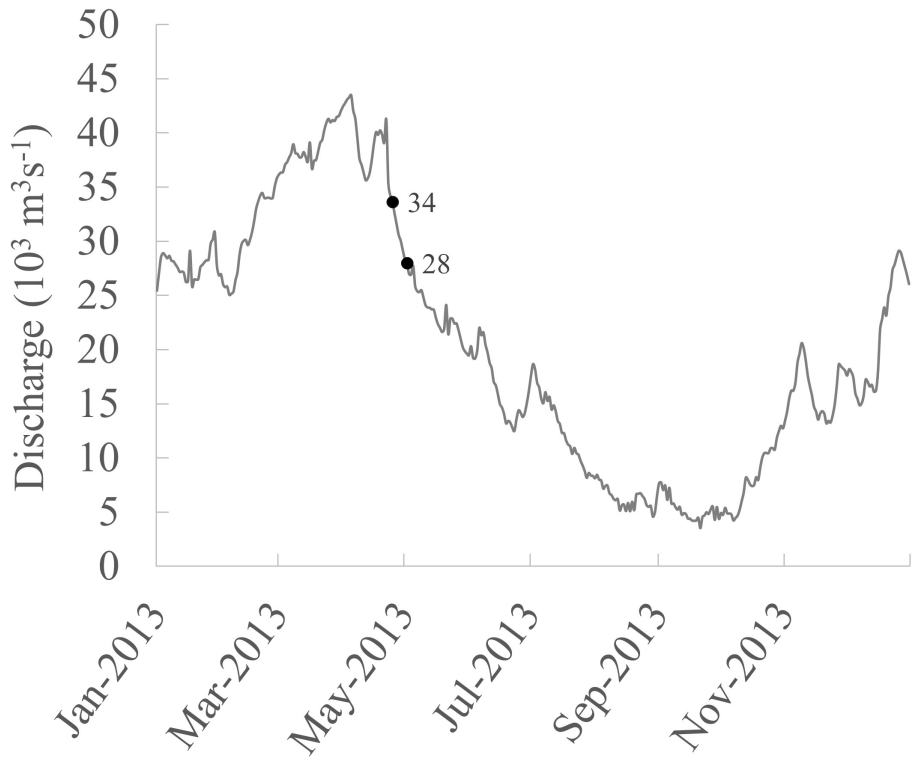

FIGURE 2 | Daily discharge in 2013 measured at station 15400000 (Brazilian National Water Agency–ANA, available at www.snirh.gov.br/hidroweb/). The station is located downstream of the Santo Antônio dam in front of Porto Velho. The numbers in the figure indicate the discharge measured at the first and last days of sampling.

77, 99, and 111, totalizing 16 measurements over each vial's incubation period. Samples were taken after injecting, mixing, and withdrawing 2 ml of N_2 in the headspace. Calculations to correct for the sampling dilution were done for each time step of the analysis. Specific rates of CH_4 production for each vial were calculated in a moving window of four measurements along the total incubation time and accepted when the $R^2 > 0.7$ and the linear regression model $p < 0.001$. After that, the potential CH_4 production rate expressed by the production by dry weight of sediment incubated ($\mu g\ CH_4\ g_{dw}^{-1}\ d^{-1}$) was assumed to be the maximal production observed. Gas samples were analyzed for CH_4 concentrations with gas chromatography (7890A, Agilent Technologies, Santa Clara, CA, United States). Triplicate aliquots of the homogenized sediments were dried for 48 h at 50°C for water content determination and grounded for carbon and nitrogen concentrations analysis to assess sediment's carbon to nitrogen ratio (C:N). Carbon and nitrogen were analyzed using a Delta Plus, ThermoQuest−Finnigan.

Water Concentrations and CH_4 Flux Calculation

Triplicate samples for CH_4 concentration were taken from three different depths: surface (30 cm below the surface), mid-depth (50% of the total depth), and near the bottom (80% of the total depth) at sites 1 and 2, and surface and bottom depths at site 3 (**Table 1**). Approximately 1 km upstream Site 3, there was a small (∼4 m wide and 0.5 m deep) outlet draining water from the flooded forest on the left side of the river where samples for CH_4 concentration and stable isotope analysis were collected. Water samples were collected in 1 L bottles, and dissolved CH_4 was determined by headspace extraction and calculated using Henry's Law adjusted for temperature according to Wiesenburg and Guinasso (1979). We used a mass balance based on the common gas law for correcting the addition of atmospheric CH_4 while creating the headspace by simultaneously removing 60 ml of water and adding 60 ml of air using a rubber stopper with two tubing and valves where the two syringes were attached to make the transfer. The total CH_4 flux from the river was measured using floating chambers while drifting with the river at the same time and locations as the sample collection described above. Fluxes were measured using seven light-weight polypropylene floating chambers (Galfalk et al., 2013), covering an area of 0.041 m^2 and with 6.03 L of headspace when deployed, attached with a line 1.5 m apart from each other and to the boat. Deployments were done drifting for approximately 30 min. After the deployment time, chambers were slowly pulled back close to the boat, and final samples were taken one by one. Air 10 cm above the water surface and final samples withdrawn from chambers were done using 60 ml syringes with two-way valves. All concentration and flux samples were immediately transferred to 20 ml glass vials pre-filled with salt solution capped with a 10 mm thick massive

TABLE 1 | Characterization of the sampled sites along the cross-channel measurements.

	Site 1			Site 2			Site 3				
Cross-channel	**A**	**C**	**E**	**A**	**C**	**E**	**A**	**B**	**C**	**D**	**E**
Depth (m)	26.8	43.3	25.6	16.8	18.0	17.9	33.8	20.5	17.8	19.3	11.2
Drifting speed (Km h^{-1})	1.9	4.7	0.4	3.9	5.4	3.3	5.2	6.7	5.7	4.3	5.0
Wind speed m s^{-1}	1.4	1.0	0.5	1.6	1.5	0.7	2.6	4.2	2.6	3.1	2.2
Water temp °C	27.5	28.2	27.7	27.8	27.9	27.7	27.1	27.1	27.2	27.1	27.2
Air temp °C	29.8	30.1	31.1	29.8	29.1	29.3	27.0	27.8	29.7	28.1	28.0
Conductivity (μS cm^{-1})	59.7	58.9	62.3	61.1	61.1	60.0	60.5	60.9	60.2	60.1	52.4
OD (% sat)	76.6	78.2	76.9	108.9	113.9	102.1	90.2	94.2	92.6	90.6	82.6
OD (mg L^{-1})	6.1	6.1	5.8	8.6	9.0	8.0	7.2	7.5	7.4	7.2	6.6
pH	6.3	6.0	6.4	6.5	6.5	6.5	6.4	6.2	6.5	6.5	6.3

All measurements other than drifting speed were done keeping the boat stationary at the starting point before we start to drift.

blue butyl rubber stoppers and an aluminum crimp seal–the salt solution was replaced by the gas sample yielding intact gas samples suitable for storage until analysis (Bastviken et al., 2010). Concentrations of CH_4 in the chambers and dissolved in the water were analyzed using a GC (Shimadzu 14A), interfaced with a flame ionization detector.

Our flux measurements captured the total fluxes (F_T), which was calculated using a linear estimate of the change in the number of mols of CH_4 inside the chambers based on the equation according to Bastviken et al. (2004):

$$F_T = \frac{(dCH_4) \cdot (V)}{R \cdot T \cdot A \cdot t}, \quad (1)$$

where, dCH_4 is the difference between final and initial partial pressure of CH_4 inside the chambers (μatm), V is the chamber volume (L), R is the ideal gas constant (0.082056 L atm K^{-1} mol^{-1}), T is the temperature (K), A is the area covered by the chamber (m^2), and t is the chamber deployment time (days). The diffusive flux equation was used to estimate the piston velocity, which was normalized into k_{600} according to Eqs 2, 3, respectively.

$$F_D = k \cdot (C_w - C_f), \quad (2)$$

where F_D is the diffusive flux (mol m^{-2} d^{-1}), k the piston velocity (m d^{-1}), C_w is the concentration of CH_4 measured in the water (mol m^3), and C_{fc} is the CH_4 concentration in the water at equilibrium with the CH_4 partial pressure in the floating chamber (Cole and Caraco, 1998). After estimating k, it was normalized to k_{600} values using the following equation (Jahne et al., 1987; Wanninkhof, 1992):

$$k_{600} = k_T \cdot \left(\frac{600}{Sc_T}\right)^{-0.5}, \quad (3)$$

where k_T is the measured k value at *in situ* temperature (T), Sc_T is the Schmidt number calculated as a function of temperature (T). The two flux components' differentiation considers the distribution and variance in the apparent piston velocities normalized to k_{600}. Deploying multiple chambers allows diffusion rates to be determined by observing similar and low apparent k_{600} in different chambers where only diffusive flux is registered. When a chamber captures ebullition, the apparent k_{600} is considerably higher than other chambers deployed simultaneously. The distribution of the apparent k_{600} can be derived by dividing the k_{600} values by the minimum value observed in each measurement with the seven chambers. Normalization to the lower apparent k in each group of measurements allows combining all groups of measurements in the analysis of the data distribution to separate the apparent k values being close to the minimum value (signaling primarily diffusive flux) and those with more variable and higher apparent k values (indicating ebullition). The binned distribution frequency considering all chambers and measurements was used to determine a threshold that separates diffusion from ebullition. Here we used a threshold of 8.5. This high threshold was needed due to the large heterogeneity of apparent k within and between sites caused by different water turbulence levels. When ebullition was recognized in a specific chamber, we subtracted the total flux by the mean diffusive flux from the other chambers deployed at the same time to obtain the ebullitive flux.

Analysis of variance (ANOVA) for cross-channel and site comparison was done after log transformation of the data to meet the statistical analysis assumptions. Each chamber in a specific deployment period was considered as an independent measurement. Statistical analyses were all done using R (R Core Team, 2019).

CH_4 Isotopic Composition and Fraction of Oxidation

The isotopic composition of dissolved CH_4 (δ^{13}-CH_4 and δD-CH_4) in river water was determined using aliquots of the same headspace samples used for water concentration analysis. Atmospheric air was used to make the headspace extraction, and thus it was also analyzed for stable isotopes for further corrections. CH_4 trapped in the sediments was also characterized for stable isotopes. Bubbles from the sediment were collected using an inverted funnel after physically disturbing the sediment. Stable isotope analysis was carried out at the UC Davis Stable Isotope Facility using a ThermoScientific Precon concentration unit interfaced to a ThermoScientific Delta V Plus isotope

ratio mass spectrometer (ThermoScientific, Bremen, Germany). Isotopic data are reported as δ permil units (%) relative to the international standards Vienna PeeDee Belemnite (V-PDB) for carbon and Vienna-Standard Mean Ocean Water (V-SMOW) for hydrogen.

The range of the fraction of CH_4 oxidation was estimated based on the maximum and minimum values obtained by two open system models for ^{13}C isotopic fractionation previously used by Happell et al. (1994) (Eq. 4) and Tyler et al. (1997) (Eq. 5), as follows:

$$f_1 = (\delta_{sw} - \delta_b) / ((\alpha - 1) \times 1000) \quad (4)$$

$$f_2 = (\delta_b - \delta_{sw}) / ((\delta_{sw} + 1000)(1 - \alpha)) \quad (5)$$

Where f is the total fraction of CH_4 oxidized (%) from Eqs 1, 2, before emission to the atmosphere. δ_b and δ_{sw} are the δ^{13}-CH_4 values for stirred bubbles from sediment and at the surface water (30 cm), respectively, and α is the isotopic fractionation factor. Due to the lack of an α value specifically for the Amazon, we choose to use a range of fractionation factors (1.025 and 1.033) from paddy environments that were obtained with temperatures between 26 and 28°C (Tyler et al., 1997; Zhang et al., 2013). To our knowledge, this is the most similar environment where the fractionation factor for methane oxidation has been determined. Thus the range reported here consists of the lowest and highest fractionation based on the two models' results using the two different α values.

The Madeira River channel mainly consists of coarse sand, and adequate areas for CH_4 production in the original river channel are constrained to the shore where fine sediments and organic matter accumulate due to vegetation in the shallow margins or the flooded soils by the reservoir. As input to the models, we assumed that the δ^{13}C-CH_4 signatures found in the bubbles trapped in the sediments near the shore represent the source endmember and the δ^{13}C-CH_4 on the surface of the water column were assumed to represent the pool of oxidized CH_4 leaving the system due to degassing. The ecosystem oxidation estimations based on the δ^{13}-CH_4 of the dissolved CH_4 consider that the CH_4 can travel and be consumed while being transported downstream (Sawakuchi et al., 2016). Thus, considering a point source adding CH_4 into the water column, the gross oxidation would increase as a function of the source's distance. Hence, the method used integrates the CH_4 dynamics across a river stretch upstream of the sampling points.

The sediment CH_4 bubbles collected in Site 1 represent the signal for CH_4 produced in the reservoirs' littoral sediment. The shoreline downstream the dam had to have the soil removed and protected with rocks to avoid erosion caused by the high water velocity, preventing us from collecting bubbles from the sediment at Site 2. Methane production in this area is potentially reduced or absent due to these conditions. Therefore, we assumed that the CH_4 available in Site 2 came from the reservoir, and the same δ_b was used. Sediment bubbles sampled approximately 3 km upstream of Site 3 represent the signal of the CH_4 produced in the sediment on the shore of the natural flowing river.

RESULTS

Potential Production of CH_4 and C:N

The highest potential CH_4 production rate was observed in the reservoirs' littoral sediment at Site 1 (0.025 ± 0.023 μg CH_4 g_{dw}^{-1} d^{-1}) and was six times higher than the potential CH_4 production at Site's 3, the naturally flooded river shore (0.004 ± 0.002 μg CH_4 g_{dw}^{-1} d^{-1}), while the Madeira River channel bed at Site 3, dominated by sand, had negligible CH_4 production rates ($5.84 \times 10^{-6} \pm 7.47 \times 10^{-6}$ μg CH_4 g_{dw}^{-1} d^{-1}). C:N followed the same pattern, with higher values observed in the littoral sediments of Site 1, followed by the sediment in the naturally river bank in Site 3 and sand from the center of the channel at Site 3, 8.7 ± 0.4, 7.1 ± 0.27, and 4.99 ± 0.50, respectively. C:N was positively correlated with the potential CH_4 production rates (Spearman $\rho = 0.73$, p-value < 0.05).

Variation in CH_4 Concentration and Flux to the Atmosphere

During flux measurements drifting and wind speeds ranged from 0.4 to 5.7 and 0.5 to 4.2 m s^{-1}, respectively (**Table 1**). Overall, CH_4 concentrations ranged from 0.005 to 0.41 μM at Site 1, 0.005 to 1.2 μM at Site 2, and 0.009 to 0.09 μM at Site 3, with variable patterns of dissolved CH_4 concentrations along the cross-sections at different depths. The highest CH_4 concentration values were at the surface in the center of Site 2 (**Figure 3**). Although we have observed the highest CH_4 concentration in the center of Site 2 (**Figure 4** and **Table 2**), the total and diffusive CH_4 fluxes were maximal at Site 3, near the shoreline (**Table 2**). Total and diffusive fluxes and CH_4 concentrations at Site 3 followed a similar pattern, with higher CH_4 total and diffusive fluxes toward both margins. Ebullition was recognized at all sites, and maximal values were registered at Site 3, where the boat drifted over shallow areas near the shore (**Table 2**). Measurements in the reservoir (Site 1) indicate a large variability in CH_4 concentrations along the water column and across the channel (**Figure 3**). Total and diffusive CH_4 fluxes also varied across the main channel of the ROR reservoir (**Figure 4**).

We combined all data from each site for the overall comparison among sites, and the results indicate no significant difference in average concentrations between sites (ANOVA, $p = 0.85$). These values were similar to concentrations reported 1,000 km downstream near the Madeira River mouth by Sawakuchi et al. (2014). The highest overall total and diffusive flux per site were observed at Site 3 (6.74 ± 30.38 and 0.89 ± 0.31 mmol m^{-2} d^{-1}, respectively), while the lowest total and diffusive fluxes were both observed in the reservoir (0.74 ± 1.67 and 0.18 ± 0.36 mmol m^{-2} d^{-1}, respectively). The diffusive fluxes measured here correlated moderately with drifting speed (Spearman's correlation, $\rho = 0.50$, $p < 0.05$) and strongly with wind (Spearman's correlation, $\rho = 0.78$, $p < 0.001$). The similar pattern observed between sites where diffusive flux, wind and drifting speed were higher at Site 3 (**Figure 5**), indicate that turbulence attributed to a combination of higher wind and water speed may be an important driver controlling diffusive fluxes downstream the dam. Higher drifting speed occurred

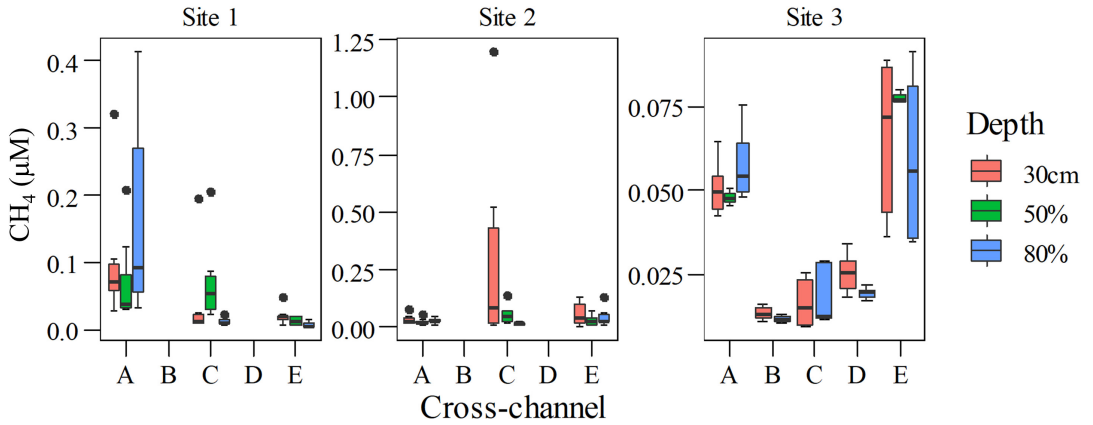

FIGURE 3 | Cross-channel profiles of dissolved CH_4 at different depths. Note that at Site 3 measurements at 50% depth were done only in site A and E. Note different values in the *y*-axis.

in the middle of the channel in all sites, while wind speed presented more variability across the channel for the different sites (**Figure 6**).

Isotopic Composition and Oxidation of CH_4

The isotopic composition of methane varied considerably between sites and across the river (**Table 2**). Site 1 presented a wide range of isotopic compositions with more depleted δ^{13}-CH_4 values observed at Site 1-A and very enriched δ^{13}-CH_4 values at Site 1-C, in the center of the channel, indicating an input of fresh CH_4 upstream along the left shore and an oxidized load in the center of the channel. δ^{13}-CH_4 values were considerably more enriched at Site 3 relative to the upstream sites, except for deep water at Site 1-C, indicating highly oxidized CH_4 along the downstream gradient. At Site 3 there was a consistent shift in the isotopic composition across the channel, with highly enriched δ^{13}-CH_4 toward the river channel's deepest zone at Site 3-A and 3-C (**Tables 1**, **2**). The fraction of oxidized CH_4 was maximal at Site 3 and in the center and right side of Site 1, where CH_4 was estimated to be nearly 100% oxidized. The lowest fraction of oxidized CH_4 was found in Site 2, especially in the channel's center and Site 1-A (**Table 2**).

DISCUSSION

Internal and Local Variability

It has been shown that CH_4 emissions and oxidation may vary in space and time within Amazonian rivers (Sawakuchi et al., 2014, 2016). Such variability is also expected in the Madeira River, and because our study covered only the falling water season and a few sites, we highlight that the findings presented here are a snapshot of the CH_4 dynamics at the early stage after reservoir construction.

Variation in water concentrations within Sites 1 and 3 (across the channel) may be related to the inflow of CH_4-rich waters from nearby flooded areas by the reservoir or naturally on river shores (Borges et al., 2015; McGinnis et al., 2016). The higher CH_4 concentration observed on the deepest point of Site 1-A (**Figure 3**), may be attributed to the dissolved input of CH_4 produced in the sediments that was the soil in pre-impoundment conditions. The lateral transport of this CH_4 from the littoral zone of the reservoir to the main channel could explain the higher concentration observed at the 50% depth of Site 1-C (**Figure 3**), which is roughly at a similar depth as the bottom of Site 1-A (**Table 1**). Apart from the large variation in CH_4 concentration observed at the surface of Site 2-C, the lower variability in CH_4 concentrations compared to Site 1 (**Figure 3**) may be attributed to the water mixing due to the passage through the spillways and turbines. During the sampling campaign, only 10% of the total installed capacity (3568 MW) was being generated (ONS, 2021). Hence, it is reasonable to consider that only a few turbines were working, and most of the water was spilled from the flood control gates located in the middle of the dam. The high O_2 saturation observed at Site 2 (**Table 1**) also indicates the large flow through the spillways causing aeration of the water. Site 3 showed greater vertical than horizontal mixing (low variability within and among depths, but some variability among sampling locations; **Figure 3**). The cross-section conditions at Site 3 are similar to previous observations in Amazonian rivers, where the concentration of CH_4 generally increases toward the shore (Richey et al., 1988; **Table 2** and **Figure 4**), indicating a lateral input of CH_4 from the seasonally flooded shores and lateral groundwater base flow to the river channel (Jones and Mulholland, 1998). Sampling was done during the falling water season when CH_4-rich water from naturally flooded areas starts to drain back into the rivers (Borges et al., 2015). Methane distributions deviated from this trend at sites 1 and 2, possibly because sampling at Site 1 may integrate CH_4 inputs from a vegetated island on the left side of the river channel upstream Site 1 (**Figure 1**) and on Site 2 because of homogenization due to mixing by the water passage through the main spillway in the center of the dam and the few turbines in operation. We observed that a high fraction of CH_4 was oxidized in all three sites, with the minimal and maximal CH_4 oxidation at Sites 2

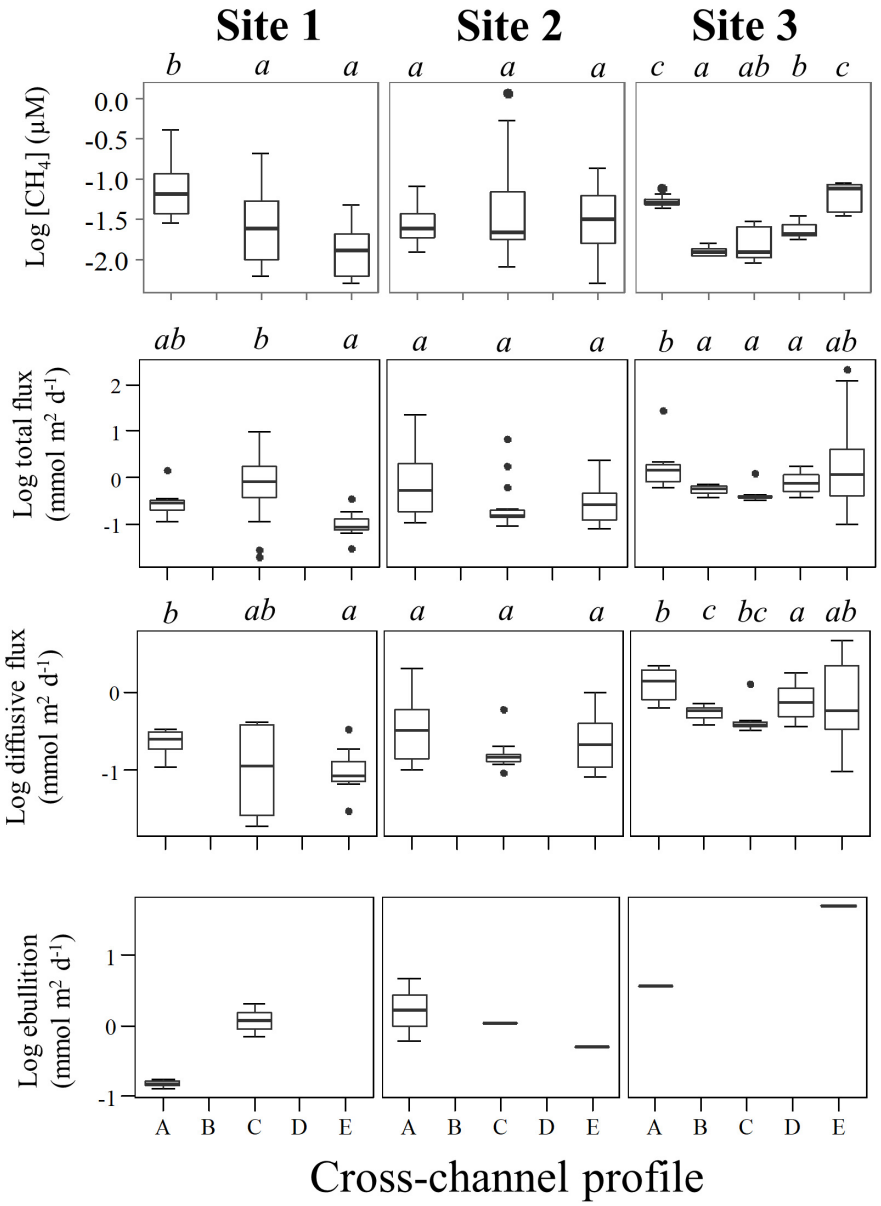

FIGURE 4 | Box-plots of the cross-channel profiles from the left bank (A) to right bank (E) of CH_4 concentration, diffusive flux, ebullition, and total flux in log scales. The boxes include the median flux and the quartile range (Q3–Q1; where Q denote quartiles). The whiskers include all data within the range (Q1–1.5(Q3–Q1)) to (Q3+1.5(Q3–Q1)). The black dots show data outside this range. Small italic letters above charts show grouping according to ANOVA, $p < 0.01$ followed by a Tukey *post-hoc* test ($p < 0.05$). Ebullition does not show grouping statistics because of the small number of occurrences, and consequently, not meeting assumptions requirements for the statistical test.

and 3, respectively (**Table 2**). The passage of water through a few turbines and the main spillway in the center of the dam might have favored a mixing of lateral water rich in CH_4 from littoral areas and tributaries near the dam. An input of CH_4 followed by a mixture at the dam would make the isotopic signature more negative, resulting in a lower fraction of CH_4 oxidation estimate as observed in Site 2. In contrast, Site 3 showed that the measured pool of CH_4 was highly oxidized, indicating the absence of a significant source area of fresh (non-oxidized) CH_4 nearby.

In the reservoir, the dam's flow control may not only increase ebullitive emissions due to water-level fluctuation but could directly affect the input of CH_4-rich waters from tributaries and bays into the main channel (Harrison et al., 2017). Due to the Madeira River's high discharge, reducing the water flow through the dam would create a flooding effect upstream of the reservoir, forcing water to flow into the bays and tributaries where CH_4 may be produced. An input of CH_4-rich water from bays and tributaries to the main channel would then be expected when the water level starts to decrease, which may have been the

TABLE 2 | Average values ± standard deviation and number of samples in the parenthesis of dissolved CH_4 concentration, total flux, diffusive flux, ebullition, δ^{13}-CH_4 signatures in the water, and sediment bubbles, and the fraction of CH_4 oxidized along the cross-sections estimated by the different open system models.

Site	Profile	[CH_4] (μM)	Total flux (mmol m^{-2} d^{-1})	Diffusive flux (mmol m^{-2} d^{-1})	Ebullition (mmol m^{-2} d^{-1})	δ^{13}-CH_4 surface water (%)	δ^{13}-CH_4 deep water (%)	δ^{13}-CH_4 bubbles (%)	Fraction oxidized [a] (Eq. 4)		Fraction oxidized [a] (Eq. 5)	
									Min	Max	Min	Max
Site 1	A	0.11 ± 0.11 (18)	0.33 ± 0.33 (13)	0.24 ± 0.08 (12)	0.09 ± 0.34 (1)	−50.85 ± 0.81	−45.23 ± 3.84	−60.87	0.39	0.51	0.41	0.54
	C	0.04 ± 0.06 (15)	1.67 ± 2.60 (13)	0.19 ± 0.18	1.46 ± 2.54 (8)	−12.06 ± 1.98	5.34		1§	1§	1§	1§
	E	0.01 ± 0.01 (17)	0.12 ± 0.09 (11)	0.12 ± 0.09	0.00	−28.73	−28.57		0.98	1§	1§	1§
Site 2	A	0.03 ± 0.02 (18)	3.11 ± 6.26 (14)	0.51 ± 0.58	2.60 ± 6.15 (4)	−36.98 ± 0.46	−38.82 ± 5.63	−60.87	0.70	0.92	0.72	0.95
	C	0.13 ± 0.29 (16)	0.75 ± 1.71 (14)	0.19 ± 0.13	0.55 ± 1.69 (2)	−59.48 ± 0.50	−30.09 ± 0.18		0.49	0.64	0.50	0.66
	E	0.05 ± 0.04 (18)	0.57 ± 0.73 (14)	0.30 ± 0.26	0.25 ± 0.65 (2)	−44.90 ± 3.92	−40.43 ± 6.52		0.55	0.73	0.58	0.76
Site 3	A	0.05 ± 0.009 (14)	3.35 ± 7.12 (13)	1.38 ± 0.57	2.01 ± 7.23 (1)	18.00 ± 0.79	11.68 ± 0.83	−53.69	1§	1§	1§	1§
	B	0.01 ± 0.002 (12)	0.55 ± 0.11 (13)	0.55 ± 0.11	0.00	–	–		–	–	–	–
	C	0.02 ± 0.007 (11)	0.45 ± 0.25 (13)	0.45 ± 0.25	0.00	15.47	20.25 ± 0.0001		1§	1§	1§	1§
	D	0.02 ± 0.005 (12)	0.85 ± 0.42 (12)	0.85 ± 0.42	0.00	–	–		–	–	–	–
	E	0.07 ± 0.02 (15)	26.5 ± 62.9 (14)	1.32 ± 1.46	24.8 ± 62.3 (3)	−10.22 ± 0.07	−9.46 ± 1.60		1§	1§	1§	1§

When SD is not presented, only one sample was taken. For ebullition, the number in parenthesis represents how many chambers received ebullition. A and E in the cross-section profile indicate measurements near the left and right margins, respectively.

[a]Range calculated using α = 1.033 and α = 1.025 from Tyler et al. (1997) and Zhang et al. (2013);

§Overestimation by the equations indicating approximately 100% oxidation.

case during our sampling campaign at the beginning of the falling water season.

Despite the widening of the channel in the reservoir would favor wind speed and gust speed, increasing the gas exchange, the highest wind speed was observed at Site 3, where the river channel was narrowest in relation to the other sites. Diffusive flux was correlated with wind speed and water velocity, and the highest diffusive flux was observed at Site 3. Similar correlation has been reported in other large rivers (Alin et al., 2011; Beaulieu et al., 2012; Sawakuchi et al., 2017).

δ^{13}-CH_4 and Methane Oxidation in the Madeira River

The average δ^{13}-CH_4 of the air over the river was −42.7 ± 0.5%, which is 3–5% more enriched than previously observed over floodplains in the Amazon (Wassmann et al., 1992). The average δ^{13}-CH_4 for bubbles in the sediment was −56.1 ± 3.4%, which is within the range of −74.6 to −41.7% already reported in Amazonian floodplains and streams (Wassmann et al., 1992; Devol et al., 1996; Moura et al., 2008). The δ^{13}-CH_4 in the water varied from −60.0 to +20.4% (**Table 2**). Available information for δ^{13}-CH_4 in the water column in aquatic environments in the Amazon ranges from −64 to −7% and −35 to −19% in the Tucuruí and Samuel Reservoirs, respectively (Lima, 2005), and from −73 to −42% for the Amazon River floodplain (Devol et al., 1988). Positive values for δ^{13}-CH_4 up to +86% were previously reported for the residual CH_4 in incubation experiments with enriched cultures of methane-oxidizing bacteria (MOB) after more than 95% of the CH_4 was consumed (Coleman et al., 1981; Feisthauer et al., 2011). However, recently, positive δ^{13}-CH_4 values were observed in other rivers and floodplain lakes in the Amazon (Sawakuchi et al., 2016; Barbosa et al., 2018). The highly positive values found in a few cases here were surprising. To ensure that there was no bias, and support that the highly enriched δ^{13}-CH_4 values found were due to biological oxidation, we also measured δD in CH_4 in a third replicate. Signatures of δD-CH_4 ranged from −289.1 to +465.8%, and a positive correlation between δ^{13}-CH_4 and δDCH_4 (Spearman rho = 0.66, $p < 0.005$) indicated bacterial oxidation of methane, according to Whiticar (1999).

At all sites, the deepwater traveling in the middle of the channel was more δ^{13}-CH_4 enriched. This pattern may be related to the fact that this mass of water in the middle receives less CH_4 from lateral flow from the river banks and flooded areas adjacent to the river and that a majority of the CH_4 oxidation occurs in well-aerated surface sediments. As discussed in Sawakuchi et al. (2016), rivers with high suspended sediment load may enhance CH_4 oxidation by transporting methanotrophs from soils. Additionally, high turbidity decreases CH_4 oxidation inhibition by light (Dumestre et al., 1999; Murase and Sugimoto, 2005). Thus, in turbid rivers such as the Madeira River, MOB may be more abundant and active. Soil MOB is shown to be attached to smaller mineral fractions and have a greater CH_4 oxidation capacity at lower CH_4 concentrations (Bender and Conrad, 1994), potentially explaining the high CH_4 oxidation and consequent low CH_4 concentrations. Furthermore, the deep and

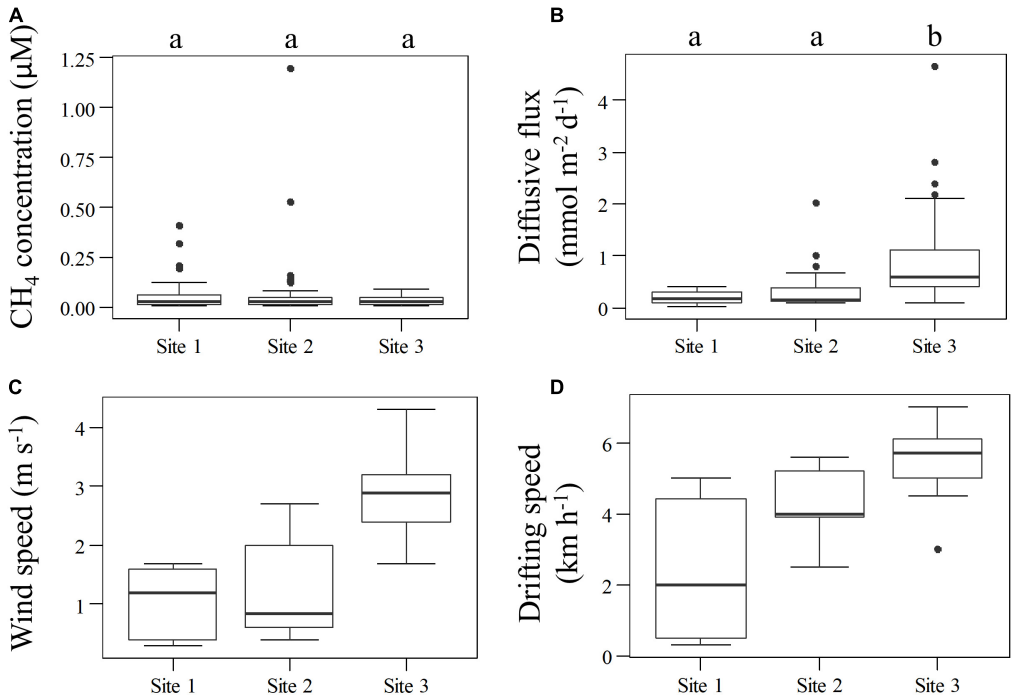

FIGURE 5 | CH_4 concentration **(A)**, diffusive flux **(B)**, wind **(C)**, and water speed **(D)** variation for each site. The small letter above CH_4 concentration and diffusive flux charts show grouping according to ANOVA, $p < 0.01$ followed by a Tukey *post-hoc* test ($p < 0.05$). Wind and drifting speed do not show grouping statistics because of the small number of measurements, and consequently, not meeting assumptions requirements for the statistical test.

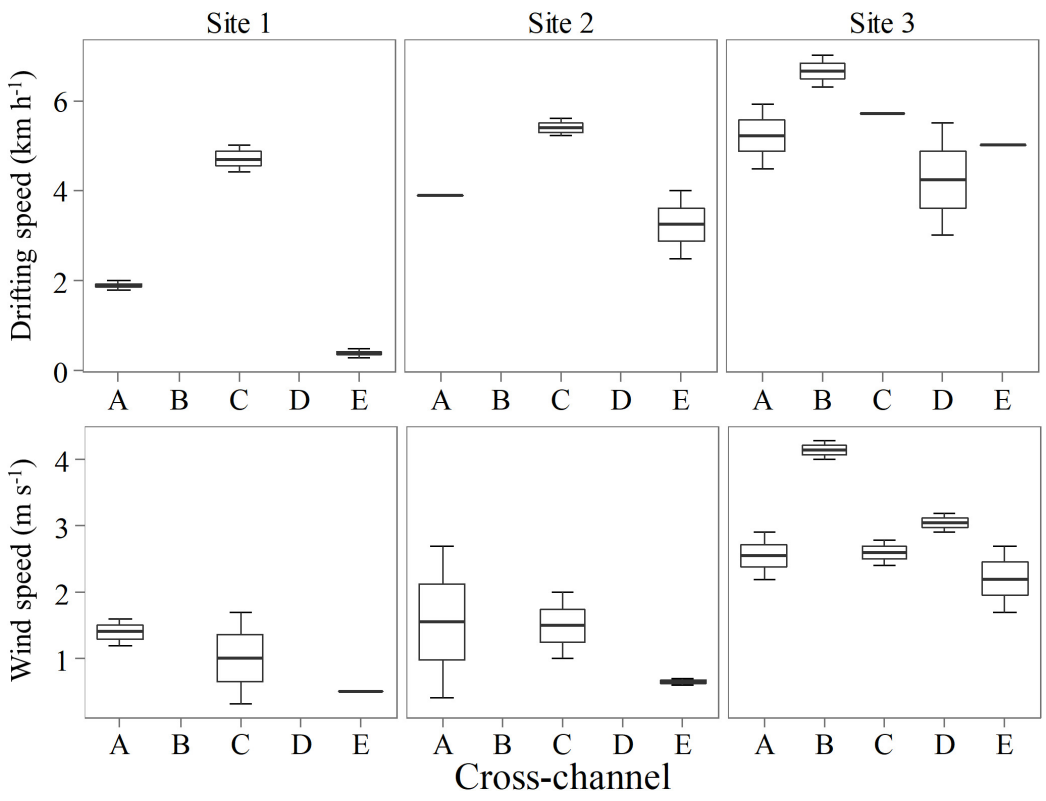

FIGURE 6 | Cross-channel variation in drifting speed of the boat and wind speed measured in two consecutive days for each site.

potentially mixed water column in the reservoir's main channel, indicated by a homogeneous temperature profile in a location in the main channel of the reservoir near Site 1 (Almeida et al., 2019a), could sustain oxygen levels in the water at the bottom and help exchange O_2 from the water into the sediment surface, potentially increasing sediment CH_4 oxidation at the sediment water interface.

Although this study was focused on the reservoir's main channel, it is important to highlight that the large drowned areas, especially in tributary valleys, can develop lake-like conditions and water column stratification (Almeida et al., 2019a). The higher water residence time in these areas allows sedimentation of fine organic sediments and may create oxygen stratification that favors CH_4 accumulation in the hypolimnion. A shallower oxic water column combined with less suspended particles for the methanotrophs to adhere to, associated with higher light penetration increasing methanotrophy inhibition, could reduce CH_4 oxidation and, consequently, increase diffusive CH_4 emissions in these areas. In the naturally flooded forest, this light inhibition may not happen due to the forest canopy cover, allowing more CH_4 oxidation than the open areas of bays and tributaries, as observed in the samples collected from the outlet upstream Site 3. Despite small in relation to the total river discharge, the input of oxidized CH_4 from the flooded forest and continued oxidation in the river channel might explain heavily oxidized CH_4 found in Site 3. However, future research is needed to assess how much oxidation happens in bays, tributaries, and naturally flooded forests.

Influence of ROR Reservoir on the CH_4 Input in the Madeira River

The isotopic approach to estimate CH_4 oxidation in running water systems provides an evaluation of the cumulative oxidation of CH_4 entering the system from various sources upstream of the sampled site. Most CH_4 oxidation may happen at the sediment-water interface with the remaining pool of dissolved CH_4 going to the water column and traveling downstream from its source, and the fraction that is oxidized will continue to increase, making the isotopic signal more enriched in ^{13}C. New sources of CH_4 along a downstream gradient would alter the *in situ* isotopic compositions, pushing it back toward more negative values. Isotopic characterization of dissolved CH_4 across Site 1 indicates the existence of source areas nearby Site 1-A. In the satellite image of the area before the reservoir (**Figure 1**), it is possible to observe a large vegetated island upstream Site 1, on the left side of the river channel, that may be the source of CH_4 to Site 1-A, explaining the difference in δ^{13}-CH_4 observed across the main channel of the reservoir.

The decrease in the δ^{13}-CH_4 variability in the dissolved CH_4 at Site 2 may indicate a homogenization, by the water passage through the turbines and spillways, of the new CH_4 produced in the areas flooded by the reservoir and the dissolved and more oxidized load from the upstream river observed in the center of the channel. Degassing from traditional dams and just downstream of their turbines is already recognized as an important pathway of CH_4 emissions to the atmosphere (Deemer et al., 2016). ROR reservoirs are not expected to have a stratified water column in the main channel at the dam where CH_4 could accumulate and be degassed at the turbines and spillways. DelSontro et al. (2016) did not observe a difference in the CH_4 concentration before and after the dam, indicating negligible degassing in a temperate ROR reservoir. Like DelSontro et al. (2016), our data do not indicate a significant difference in concentration between Site 1 and Site 2, suggesting negligible degassing at the dam. However, we highlight that our data is a snapshot of the conditions in only one season during the beginning of the operations.

The original river properties remained similar in the main channel of the reservoir after the dam installation (Almeida et al., 2019a; Rivera et al., 2019), indicating that conditions for CH_4 oxidation may follow the same trend as non-disturbed rivers where higher CH_4 oxidation was observed in the high water season in contrast with the low water season (Sawakuchi et al., 2016). The falling water season may be a critical hydrologic season regarding GHG input and CH_4 oxidation in rivers and ROR reservoirs. In this period, water from natural floodplains and drowned tributaries in reservoirs feed the main river channel bringing dissolved gases from these potential source areas to the deep and oxic main channel where CH_4 can be oxidized.

The higher potential CH_4 production in the areas flooded by the reservoir is related to the amount and quality of the organic matter in the reservoirs' littoral sediment assessed by the C:N values. The CH_4 production rate at Site 1 was within the range of the CH_4 production rate (0.019–0.033 CH_4 $g_{sed}{}^{-1}$ d^{-1}) in the upper layers (first 5 cm and next 10 cm, respectively) of the primary forest soil next to the Petit Saut reservoir. The CH_4 production observed at the shore of Site 3 was similar to the CH_4 production for the 10-year-old flooded soils in the Petit Saut reservoir's littoral zone in French Guiana, which varied from 0.003 to 0.134 CH_4 $g_{sed}{}^{-1}$ d^{-1} (Guerin et al., 2008). The high production rate of CH_4 observed upstream of the dam can sustain large emissions through ebullition over shallow flooded lands. However, ebullition is often underestimated by measurements using floating chambers due to episodic emissions. Furthermore, flux measurements were done over the river channel, and despite ebullition was observed in the channel, most of the ebullitive release would happen over the shallow flooded areas in bays and tributaries. Our data suggest input from the reservoir's flooded areas, although it did not increase the total and diffusive fluxes in the main channel or downstream in relation to the undisturbed river (Site 3).

Our study should be considered as a snapshot of the initial conditions of the main channel of the reservoir and a more extensive investigation of total reservoir impacts on CH_4 emissions with higher spatial and temporal coverage is still needed. The oxidation appears to play an essential role in reducing the diffusive share of the Madeira River emissions during the falling water season, maintaining low levels of CH_4 in the river channel water, and consequently having lower CH_4 emissions to the atmosphere. However, it is important to highlight that CH_4 oxidation varies among seasons and between rivers (Sawakuchi et al., 2016), and our results may only be valid for this specific study case. Although this ecosystem naturally oxidizes a significant fraction of methane before its

release to the atmosphere, turbulent conditions caused by the hydropower turbines and spillways can briefly bypass this process, releasing a portion of the CH_4 to the atmosphere that may have otherwise been oxidized further downstream. The studied reservoir and downstream river was at the early stage of operation, and, as such, the emission pathways and drowned tributaries must be further examined to inform future decisions concerning hydropower development in the region. This study brings forward the insufficient knowledge about the processes controlling the carbon cycle, especially CH_4 dynamics in large ROR reservoirs. Resolving the complex impacts of large tropical ROR hydroelectric reservoirs on CH_4 dynamics is essential for determining hydropower's net impact on regional and global-scale carbon budgets.

DATA AVAILABILITY STATEMENT

The original contributions presented in the study are included in the article or in the dataset supplemented, further inquiries can be directed to the corresponding author/s.

AUTHOR CONTRIBUTIONS

HS, DB, and AE-P formulated the study. HS, NW, and JR design the river sampling strategy and hydrological information. HS organized overall field logistics and executed the sampling. HS and PC performed the analysis. All authors contributed to data interpretation and critically revised the manuscript for final submission.

FUNDING

This study was supported by FAPESP, Grants 2011/14502-2, 2012/17359-9, 12/51187-0, 2014/21564-2, 2015/09187-1, 2018/18491-4, and NSF DEB 1754317, Swedish Research Council VR grants 2012-00048 and 2016-04829, STINT grant 2012-2085, and the European Research Council (ERC) grant METLAKE 725546. AE-P was a research fellow from CNPq and funded by a "Cientista do Nosso Estado" grant from FAPERJ.

ACKNOWLEDGMENTS

We thank Maria Victoria R. Ballester, Wanderley Rodrigues Bastos, and Alex V. Krusche for the use of their laboratory facilities, Lena Lundman, Henrik Reyier, Alexandra Montebello, and Dario Pires de Carvalho for lab and fieldwork assistance, at the University of São Paulo, Linköping University, and the Federal University of Rondônia.

SUPPLEMENTARY MATERIAL

The Supplementary Material for this article can be found online at: https://www.frontiersin.org/articles/10.3389/fenvs.2021.655455/full#supplementary-material

REFERENCES

Alin, S. R., Rasera, M. d. F. F. L., Salimon, C. I., Richey, J. E., Holtgrieve, G. W., et al. (2011). Physical controls on carbon dioxide transfer velocity and flux in low-gradient river systems and implications for regional carbon budgets. *J. Geophys. Res. Biogeosci.* 116, 1–17.

Almeida, R. M., Hamilton, S. K., Rosi, E. J., Arantes, J. D., Barros, N., Boemer, G., et al. (2019a). Limnological effects of a large Amazonian run-of-river dam on the main river and drowned tributary valleys. *Sci. Rep.* 9:16846.

Almeida, R. M., Shi, Q. R., Gomes-Selman, J. M., Wu, X. J., Xue, Y. X., Angarita, H., et al. (2019b). Reducing greenhouse gas emissions of Amazon hydropower with strategic dam planning. *Nat. Commun.* 10:4281.

Barbosa, P. M., Farjalla, V. F., Melack, J. M., Amaral, J. H. F., da Silva, J. S., and Forsberg, B. R. (2018). High rates of methane oxidation in an Amazon floodplain lake. *Biogeochemistry* 137, 351–365. doi: 10.1007/s10533-018-0425-2

Barros, N., Cole, J. J., Tranvik, L. J., Prairie, Y. T., Bastviken, D., Huszar, V. L. M., et al. (2011). Carbon emission from hydroelectric reservoirs linked to reservoir age and latitude. *Nat. Geosci.* 4, 593–596. doi: 10.1038/ngeo1211

Bastviken, D., Cole, J., Pace, M., and Tranvik, L. (2004). Methane emissions from lakes: dependence of lake characteristics, two regional assessments, and a global estimate. *Global Biogeochem. Cycles* 18, Gb4009. doi: 10.1029/2004gb002238

Bastviken, D., Santoro, A. L., Marotta, H., Pinho, L. Q., Calheiros, D. F., Crill, P., et al. (2010). Methane emissions from pantanal, South America, during the low water season: toward more comprehensive sampling. *Environ. Sci. Technol.* 44, 5450–5455. doi: 10.1021/es1005048

Beaulieu, J. J., Shuster, W. D., and Rebholz, J. A. (2012). Controls on gas transfer velocities in a large river. *J. Geophys. Res. Biogeosci.* 117:13.

Bender, M., and Conrad, R. (1994). Methane oxidation activity in various soils and freshwater sediments: occurrence, characteristics, vertical profiles, and distribution on grain size fractions. *J. Geophys. Res. Atmos.* 99, 16531–16540. doi: 10.1029/94jd00266

Borges, A. V., Abril, G., Darchambeau, F., Teodoru, C. R., Deborde, J., Vidal, L. O., et al. (2015). Divergent biophysical controls of aquatic CO2 and CH4 in the World's two largest rivers. *Sci. Rep.* 5:15614.

Cole, J. J., and Caraco, N. F. (1998). Atmospheric exchange of carbon dioxide in a low-wind oligotrophic lake measured by the addition of SF6. *Limnol. Oceanogr.* 43, 647–656. doi: 10.4319/lo.1998.43.4.0647

Coleman, D. D., Risatti, J. B., and Schoell, M. (1981). Fractionation of carbon and hydrogen isotopes by methane-oxidizing bacteria. *Geochim. Cosmochim. Acta* 45, 1033–1037. doi: 10.1016/0016-7037(81)90129-0

de Araújo, K. R., Sawakuchi, H. O., Bertassoli, D. J. Jr., Sawakuchi, A. O., da Silva, K. D., Vieira, T. B., et al. (2019). Carbon dioxide (CO2) concentrations and emission in the newly constructed Belo Monte hydropower complex in the Xingu River, Amazonia. *Biogeosciences* 16, 3527–3542. doi: 10.5194/bg-16-3527-2019

de Faria, F. A. M., Jaramillo, P., Sawakuchi, H. O., Richey, J. E., and Barros, N. (2015). Estimating greenhouse gas emissions from future Amazonian hydroelectric reservoirs. *Environ. Res. Lett.* 12, 24019–24019.

Deemer, B. R., Harrison, J. A., Li, S. Y., Beaulieu, J. J., Delsontro, T., Barros, N., et al. (2016). Greenhouse gas emissions from reservoir water surfaces: a new global synthesis. *Bioscience* 66, 949–964. doi: 10.1093/biosci/biw117

Delsontro, T., McGinnis, D. F., Sobek, S., Ostrovsky, I., and Wehrli, B. (2010). Extreme methane emissions from a swiss hydropower reservoir: contribution from bubbling sediments. *Environ. Sci. Technol.* 44, 2419–2425. doi: 10.1021/es9031369

DelSontro, T., McGinnis, D. F., Wehrli, B., and Ostrovsky, I. (2015). Size does matter: importance of large bubbles and small-scale hot spots for methane transport. *Environ. Sci. Technol.* 49, 1268–1276. doi: 10.1021/es5054286

DelSontro, T., Perez, K. K., Sollberger, S., and Wehrli, B. (2016). Methane dynamics downstream of a temperate run-of-the-river reservoir. *Limnol. Oceanogr.* 61, S188–S203.

Devol, A. H., Richey, J. E., Clark, W. A., King, S. L., and Martinelli, L. A. (1988). Methane emissions to the troposphere from the Amazon floodplain. *J. Geophys. Res. Atmos.* 93, 1583–1592. doi: 10.1029/jd093id02p01583

Devol, A. H., Richey, J. E., King, S. L., Lansdown, J., and Martinelli, L. A. (1996). Seasonal variation in the ^{13}C-CH_4 of Amazon floodplain waters. *Mitt. Int. Vereinigung Limnol.* 25, 173–178. doi: 10.1080/05384680.1996.11904078

dos Santos, M. A., Damazio, J. M., Rogerio, J. P., Amorim, M. A., Medeiros, A. M., Abreu, J. L. S., et al. (2017). Estimates of GHG emissions by hydroelectric reservoirs: the Brazilian case. *Energy* 133, 99–107. doi: 10.1016/j.energy.2017.05.082

Dumestre, J. F., Guezennec, J., Galy-Lacaux, C., Delmas, R., Richard, S., and Labroue, L. (1999). Influence of light intensity on methanotrophic bacterial activity in Petit Saut Reservoir, French Guiana. *Appl. Environ. Microbiol.* 65, 534–539. doi: 10.1128/aem.65.2.534-539.1999

Feisthauer, S., Vogt, C., Modrzynski, J., Szlenkier, M., Kruger, M., Siegert, M., et al. (2011). Different types of methane monooxygenases produce similar carbon and hydrogen isotope fractionation patterns during methane oxidation. *Geochim. Cosmochim. Acta* 75, 1173–1184. doi: 10.1016/j.gca.2010.12.006

Filizola, N., and Guyot, J. L. (2009). Suspended sediment yields in the Amazon basin: an assessment using the Brazilian national data set. *Hydrol. Process.* 23, 3207–3215. doi: 10.1002/hyp.7394

Gagnon, L., and van de Vate, J. F. (1997). Greenhouse gas emissions from hydropower - The state of research in 1996. *Energy Policy* 25, 7–13. doi: 10.1016/s0301-4215(96)00125-5

Galfalk, M., Bastviken, D., Fredriksson, S., and Arneborg, L. (2013). Determination of the piston velocity for water-air interfaces using flux chambers, acoustic Doppler velocimetry, and IR imaging of the water surface. *J. Geophys. Res. Biogeosci.* 118, 770–782. doi: 10.1002/jgrg.20064

Gerlak, A. K., Saguier, M., Mills-Novoa, M., Fearnside, P. M., and Albrecht, T. R. (2020). Dams, Chinese investments, and EIAs: a race to the bottom in South America? *Ambio* 49, 156–164. doi: 10.1007/s13280-018-01145-y

Guerin, F., Abril, G., de Junet, A., and Bonnet, M. P. (2008). Anaerobic decomposition of tropical soils and plant material: implication for the CO2 and CH4 budget of the Petit Saut Reservoir. *Appl. Geochem.* 23, 2272–2283. doi: 10.1016/j.apgeochem.2008.04.001

Happell, J. D., Chanton, J. P., and Showers, W. S. (1994). The influence of methane oxidation on the stable isotopic composition of methane emitted from Florida swamp forests. *Geochim. Cosmochim. Acta* 58, 4377–4388. doi: 10.1016/0016-7037(94)90341-7

Harrison, J. A., Deemer, B. R., Birchfield, M. K., and O'Malley, M. T. (2017). Reservoir water-level drawdowns accelerate and amplify methane emission. *Environ. Sci. Technol.* 51, 1267–1277. doi: 10.1021/acs.est.6b03185

Jahne, B., Munnich, K. O., Bosinger, R., Dutzi, A., Huber, W., and Libner, P. (1987). On the parameters influencing air-water gas exchange. *J. Geophys. Res. Oceans* 92, 1937–1949. doi: 10.1029/jc092ic02p01937

Jones, J. B., and Mulholland, P. J. (1998). Methane input and evasion in a hardwood forest stream: effects of subsurface flow from shallow and deep pathways. *Limnol. Oceanogr.* 43, 1243–1250. doi: 10.4319/lo.1998.43.6.1243

Latrubesse, E. M., Stevaux, J. C., and Sinha, R. (2005). Tropical rivers. *Geomorphology* 70, 187–206.

Leite, N. K., Krusche, A. V., Ballester, M. V. R., Victoria, R. L., Richey, J. E., and Gomes, B. M. (2011). Intra and interannual variability in the Madeira River water chemistry and sediment load. *Biogeochemistry* 105, 37–51. doi: 10.1007/s10533-010-9568-5

Lima, I. B. T. (2005). Biogeochemical distinction of methane releases from two Amazon hydroreservoirs. *Chemosphere* 59, 1697–1702. doi: 10.1016/j.chemosphere.2004.12.011

Mallia, E., and Lewis, G. (2013). Life cycle greenhouse gas emissions of electricity generation in the province of Ontario, Canada. *Int. J. Life Cycle Assess.* 18, 377–391. doi: 10.1007/s11367-012-0501-0

Marotta, H., Pinho, L., Gudasz, C., Bastviken, D., Tranvik, L. J., and Enrich-Prast, A. (2014). Greenhouse gas production in low-latitude lake sediments responds strongly to warming. *Nat. Clim. Change* 4, 467–470. doi: 10.1038/nclimate2222

McGinnis, D. F., Bilsley, N., Schmidt, M., Fietzek, P., Bodmer, P., Premke, K., et al. (2016). Deconstructing methane emissions from a small northern european river: hydrodynamics and temperature as key drivers. *Environ. Sci. Technol.* 50, 11680–11687. doi: 10.1021/acs.est.6b03268

Moura, J. M. S., Martens, C. S., Moreira, M. Z., Lima, R. L., Sampaio, I. C. G., Mendlovitz, H. P., et al. (2008). Spatial and seasonal variations in the stable carbon isotopic composition of methane in stream sediments of eastern Amazonia. *Tellus B* 60, 21–31. doi: 10.1111/j.1600-0889.2007.00322.x

Murase, J., and Sugimoto, A. (2005). Inhibitory effect of light on methane oxidation in the pelagic water column of a mesotrophic lake (Lake Biwa, Japan). *Limnol. Oceanogr.* 50, 1339–1343. doi: 10.4319/lo.2005.50.4.1339

ONS (2021). *Operador Nacional do Sistema Elétrico*. Available online at: http://www.ons.org.br/ (acessed february 23, 2021).

R Core Team (2019). *R: A Language and Environment for Statistical Computing*. Vienna: R Foundation for Statistical Computing.

Richey, J. E., Devol, A. H., Wofsy, S. C., Victoria, R., and Riberio, M. N. G. (1988). Biogenic gases and the oxidation and reduction of carbon in Amazon river and floodplain waters. *Limnol. Oceanogr.* 33, 551–561. doi: 10.4319/lo.1988.33.4.0551

Rivera, I. A., Cardenas, E. A., Espinoza-Villar, R., Espinoza, J. C., Molina-Carpio, J., Ayala, J. M., et al. (2019). Decline of fine suspended sediments in the madeira river Basin (2003-2017). *Water* 11:514. doi: 10.3390/w11030514

Sawakuchi, H., Neu, V., Ward, N., Barros, MdL, Valerio, A., Gagne-Maynard, W., et al. (2017). Carbon dioxide emissions along the lower Amazon River. *Front. Mar. Sci.* 4:76. doi: 10.3389/fmars.2017.00076

Sawakuchi, H. O., Bastviken, D., Sawakuchi, A. O., Krusche, A. V., Ballester, M. V. R., and Richey, J. E. (2014). Methane emissions from Amazonian Rivers and their contribution to the global methane budget. *Global Change Biol.* 20, 2829–2840. doi: 10.1111/gcb.12646

Sawakuchi, H. O., Bastviken, D., Sawakuchi, A. O., Ward, N. D., Borges, C. D., Tsai, S. M., et al. (2016). Oxidative mitigation of aquatic methane emissions in large Amazonian rivers. *Global Change Biol.* 22, 1075–1085. doi: 10.1111/gcb.13169

Tyler, S. C., Bilek, R. S., Sass, R. L., and Fisher, F. M. (1997). Methane oxidation and pathways of production in a Texas paddy field deduced from measurements of flux, delta C-13, and delta D of CH4. *Global Biogeochem. Cycles* 11, 323–348. doi: 10.1029/97gb01624

Wanninkhof, R. (1992). Relationship betwenn wind-speed and gas-exchange over the ocean. *J. Geophys. Res. Oceans* 97, 7373–7382. doi: 10.1029/92jc00188

Wassmann, R., Thein, U. G., Whiticar, M. J., Rennenburg, H., Seiler, W., and Junk, W. J. (1992). Methane emissions from the Amazon Floodplain: characterization of production and transport. *Global Biogeochem. Cycles* 6, 3–13. doi: 10.1029/91gb01767

Wehrli, B. (2011). Renewable but not carbon-free. *Nat. Geosci.* 4, 585–586.

Whiticar, M. J. (1999). Carbon and hydrogen isotope systematics of bacterial formation and oxidation of methane. *Chem. Geol.* 161, 291–314. doi: 10.1016/s0009-2541(99)00092-3

Wiesenburg, D. A., and Guinasso, N. L. (1979). Equilibrium solubilities of methane, carbon-monoxide, and hydrogen in water and sea-water. *J. Chem. Eng. Data* 24, 356–360. doi: 10.1021/je60083a006

Zarfl, C., Lumsdon, A. E., Berlekamp, J., Tydecks, L., and Tockner, K. (2015). A global boom in hydropower dam construction. *Aquat. Sci.* 77, 161–170. doi: 10.1007/s00027-014-0377-0

Zhang, G. B., Ji, Y., Ma, J., Liu, G., Xu, H., and Yagi, K. (2013). Pathway of CH_4 production, fraction of CH_4 oxidized, and ^{13}C isotope fractionation in a straw-incorporated rice field. *Biogeosciences* 10, 3375–3389. doi: 10.5194/bg-10-3375-2013

Conflict of Interest: The authors declare that the research was conducted in the absence of any commercial or financial relationships that could be construed as a potential conflict of interest.